Tuijin Jishu/Journal of Propulsion Technology
ISSN: 1001-4055
Vol. 45 No. 1 (2024)

A Magnetohydrodynamics Casson Nanofluid Flow Induced by Three Dimensional Permeable Stretching Surface: A Mathematical Approach

Saloni Gupta[1,*], Sanjay Kumar[2], Parmod Kumar Sharma[2], Chinta Mani Tiwari[1]
[1]*Maharishi School of Science, Maharishi School of Information Technology, Lucknow, UP-226013, India*
[2]*Department of Applied Sciences, KIET Group of Institutions, Ghaziabad, UP, India*
[*]*Corresponding author: Saloni Gupta*

Abstract: The present study describes the 3D magnetohydrodynamic flow over a permeable stretched surface in the presence of nanoparticles in Casson fluid. Extended Buongiorno's replica has been implemented in the current research. To study the nanofluid model, Brownian motion and thermophoresis impacts are used in recent research. Similarity solutions are implemented to get the final set of ODE's. To solve the system of equations, RKF algorithm has been used to calculate numerical results by following Shooting technique using ODE45 solver. The outcomes are computed using the MATLAB software. The motive behind to do this research is to analyze the impact of controlling fluid parameters, especially stretching ratio parameter c $(0 \leq c \leq 8)$, Lewis number Le $(1.0 \leq Le \leq 5.0)$, thermophoresis Nt $(1.0 \leq Nt \leq 3.0)$, Brownian motion Nb, Prandtl number Pr $(0.1 \leq Pr \leq 0.5)$, Casson parameter β $(0.1 \leq \beta \leq 0.9)$ over three-dimensional stretching surface. To calculate results for quantities of interest, contour plots, and tables are drawn. The final results are compared with existing literature, and a very good convergence has been noticed for the current research.

Keywords*: Casson Fluid, Shooting Method, Nanofluid, Buongiorno's Model, Chemical reaction, Three dimensional MHD flow.*

1. Introduction

The properties of nanofluids, particularly low resistivity and compelling thermo-physical qualities, are significant in research. To keep up, support, and foster mechanical items like PC, PCs, power hardware, powerful beams, and engine motors are exceptionally compelling in different modern strategies. Nanofluids have promisingly expanded their usefulness and results for industrial purposes. Examining non-Newtonian liquids has made an impressive consideration because of their escalated mechanical and designing applications. Instances of these liquids are suspensions, paints, emulsions, greases, paints, and numerous organic liquids. Recently, Shafiq et al. [1] explored the concept of nanofluid among Bioconvective Newtonian heating in the presence of chemical reaction by shooting procedure following RKF scheme. Hall and Ion effects over three-dimensional exponential stretching surfaces in non-Newtonian nanofluids were studied by Ibrahim and Anbessa [2]. Rana et al. [3] discussed the thermal convection flow by using monophasic model utilizing FEM technique. Goyal et al. [4] presented thermodiffusive effects in MHD nanofluid towards power law stretching surface by employing GFEM technique. Rana et al. [5] follows the Boussinesq approximation to discussed nonlinear flow by utilizing ANOVA. Also, three-dimensional convective MHD nanofluid flow for alumina particles was studied by Gupta et al. [6] by employing OHAM. In recent years, nanofluid flow in the presence of Magnetohydrodynamics under different physical aspects has been explored by authors [7-11].

The examination of non-Newtonian liquids has made an impressive consideration because of their escalated mechanical and designing applications. Instances of these liquids are suspensions, paints, emulsions, greases,

paints and numerous organic liquids. The regular highlights of every one of these day by day experienced items are that they don't submit to Newton's law of thickness. Consequently, these liquids are famous as non-Newtonian liquids. Accordingly, to contemplate broadening and inherent thermo-actual qualities of these intricate liquids, different liquid models have been proposed. These models are essentially called viscoelastic and inelastic liquids, polar liquids, anisotropic liquids, and miniature organized fluids. Gupta et al. [12] investigated the multiple solutions for Casson nanofluids with thermodiffusive effects along chemical reaction over 3D stretching surface by following shooting technique. Bio-convective three-dimensional slip flows in the presence of gyrotactic micro-organisms with chemically reactive non-Newtonian nanoparticles have been explored by Nayak et al. [13] by following bvp4c function in MATLAB. Ramzan et al. [14] presented 3D stretching surface for a viscoelastic nanofluid and found that temperature rises with a rise in Dufour parameter. Non-linear radiative impact on 3D surfaces in the presence of convective conditions has been analyzed by Mallikarjuna et al. [15]. Ramamoorthy and Pallavarapu [16] presented the Williamson fluid model with thermal radiation and magnetohydrodynamic flow by 3D stretching surface. Khan et al. [17] showed the impact of gyrotactic micro-organisms in Oldroyd-B nanofluids by employing theoretical treatment over an exponential surface. Recent research on non-Newtonian nanofluids in presence of MHD flow formation has been presented by the researchers in [18-25].

With all the above examinations done by different scientists and broad mechanical just as designing applications at the top of the priority list, we are therefore expecting to unfurl the meaning of three-dimensional magnetohydrodynamic flows over a permeable stretching surface in the presence of non-Newtonian nanofluid by following Buongiorno's model. RKF algorithm is used to calculate numerical results in the form of tables and graphs. In particular, the present study of various controlling parameters, especially non-Newtonian Casson fluid, chemical reaction, and nanoparticles, makes this research novel. The details of this research are planned as follows. In Section 2, the materials and methods part is introduced. The received mathematical strategy is clarified in Section 3. The entire summary with diagrams and their interpretation of various controlling fluid parameters are elucidated in section 4. Ultimately, Section 5 closes the present study and includes the central discoveries of the current investigation.

2. Materials and Methods

Three dimensional Casson nanofluid model induced by a permeable stretching surface with magnetohydrodynamic flow is considered. In this model, thermophoresis and Brownian motion impact of nanofluid have been incorporated among stretched velocities $\boldsymbol{U_w = ax}$ and $\boldsymbol{V_w = by}$ in $\boldsymbol{x}$ and $\boldsymbol{y}$ direction serially. Governing equations are (see [26-28]):

$$\frac{\partial u}{\partial x}+\frac{\partial v}{\partial y}+\frac{\partial w}{\partial z}=0 \tag{1}$$

$$u\frac{\partial u}{\partial x}+v\frac{\partial u}{\partial y}+w\frac{\partial u}{\partial z}=\nu\left(1+\frac{1}{\beta}\right)\frac{\partial^2 u}{\partial z^2}-\left[\frac{\sigma B_0^2}{\rho}+\frac{\nu}{k_1}\left(1+\frac{1}{\beta}\right)\right]u, \tag{2}$$

$$u\frac{\partial v}{\partial x}+v\frac{\partial v}{\partial y}+w\frac{\partial v}{\partial z}=\nu\left(1+\frac{1}{\beta}\right)\frac{\partial^2 v}{\partial z^2}-\left[\frac{\sigma B_0^2}{\rho}+\frac{\nu}{k_1}\left(1+\frac{1}{\beta}\right)\right]v, \tag{3}$$

$$u\frac{\partial T}{\partial x}+v\frac{\partial T}{\partial y}+w\frac{\partial T}{\partial z}=\frac{k}{(\rho C_p)_f}\frac{\partial^2 T}{\partial z^2}+\frac{(\rho C_p)_p}{(\rho C_p)_f}\left[\frac{D_T}{T_\infty}\left(\frac{\partial T}{\partial z}\right)^2+D_B\frac{\partial T}{\partial z}\frac{\partial C}{\partial z}\right] \tag{4}$$

$$u\frac{\partial C}{\partial x}+v\frac{\partial C}{\partial y}+w\frac{\partial C}{\partial z}=\frac{D_T}{T_\infty}\frac{\partial^2 T}{\partial z^2}+D_B\frac{\partial^2 C}{\partial z^2}-K_r(C-C_\infty) \tag{5}$$

Using similarity variables (See [29]):

$$\eta = \sqrt{\frac{a}{\nu}}z, \quad \Theta(\eta) = \frac{T - T_\infty}{T_w - T_\infty}, \quad \Phi(\eta) = \frac{C - C_\infty}{C_w - C_\infty}, \quad u = axf'(\eta), \quad v = byg'(\eta)$$
$$\text{and} \quad w = -\sqrt{av}\left[f(\eta) + c\,g(\eta)\right] \tag{6}$$

Associated B.C's are:

$$\begin{aligned} &u = U_w = ax, \quad v = V_w = by \quad \text{at} \quad w = 0 \\ &T = T_w, \quad C = C_w \quad \text{at} \quad z = 0 \\ &u \to 0, \quad v \to 0, \quad T \to T_\infty, \quad C \to C_\infty \quad \text{as} \quad z \to \infty \end{aligned} \tag{7}$$

Final transformed D.E's are:

$$\left(1 + \frac{1}{\beta}\right) f''' - f'^2 + (f + cg) f'' - \left[M + K_1\left(1 + \frac{1}{\beta}\right)\right] f' = 0 \tag{8}$$

$$\left(1 + \frac{1}{\beta}\right) g''' - cg'^2 + (f + cg) g'' - \left[M + K_1\left(1 + \frac{1}{\beta}\right)\right] g' = 0 \tag{9}$$

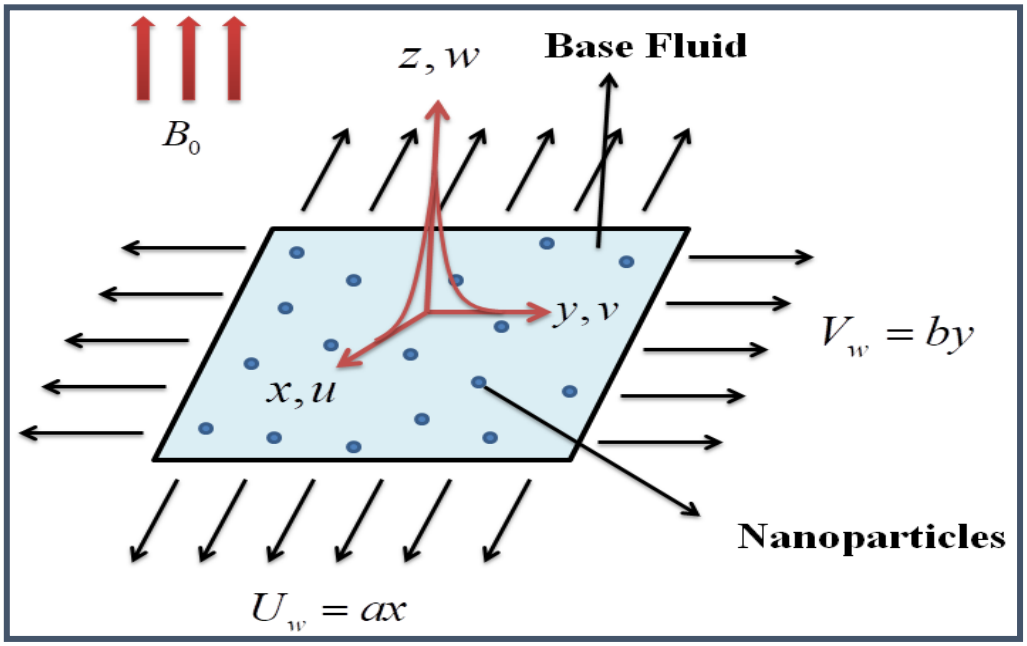

Fig. 1: Schematic diagram

$$\Theta'' + Pr\left[(f + cg)\Theta' + Nb\,\Theta'\Phi' + Nt\,\Theta'^2\right] = 0 \tag{10}$$

$$\Phi'' + Le\,Pr\,(f + c\,g)\Phi' + \left(\frac{Nt}{Nb}\right)\Theta'' - Le\,Pr\,C_r\,\Phi = 0 \tag{11}$$

Reduced B.C's are:

$$\begin{aligned} f' &= 1, \quad g' = 1, \quad \Theta(0) = 1, \quad \Phi(0) = 1 \\ f' &\to 0, \quad g' \to 0, \quad \Theta \to 0, \quad \Phi \to 0 \end{aligned} \tag{12}$$

Non-dimensional physical quantities are:

$$Sh_x = \frac{-x}{(C_w - C_\infty)} \left(\frac{\partial C}{\partial z} \right)\Big|_{z=0}, \quad Nu_x = \frac{-x}{(T_w - T_\infty)} \left(\frac{\partial T}{\partial z} \right)\Big|_{z=0}, \quad Cf_y = \frac{\tau_{yz}}{\rho U_w^{\,2}} \quad \text{and} \quad Cf_x = \frac{\tau_{xz}}{\rho U_w^{\,2}} \tag{13}$$

Reduced physical quantities of interest are:

$$Sh_x \, \mathrm{Re}_x^{-1/2} = -\Phi'(0), \; Nu_x \, \mathrm{Re}_x^{-1/2} = -\Theta'(0), \; Cf_y \, \mathrm{Re}_x^{1/2} = \left(1 + \frac{1}{\beta}\right) g''(0), \; Cf_x \, \mathrm{Re}_x^{1/2} = \left(1 + \frac{1}{\beta}\right) f''(0) \tag{14}$$

3. Numerical scheme

The arrangement of D.E's (8)-(11) with B.C's (12) are addressed mathematically by utilizing RKF procedure following the Shooting procedure by utilizing ODE45 solver in MATLAB R2014a, and these arrangement of conditions are changed over into ten 1st order D.E's as

$$\tilde{i}(1)' = \tilde{i}(2) \tag{15}$$

$$\tilde{i}(2)' = \tilde{i}(3) \tag{16}$$

$$\tilde{i}(3)' = \frac{\beta}{(1+\beta)} \left[\tilde{i}(2)^2 - \left\{ \tilde{i}(1) + c\,\tilde{i}(4) \right\} \tilde{i}(3) + M\, \tilde{i}(2) + K_1 \left(1 + \frac{1}{\beta}\right) \tilde{i}(2) \right] \tag{17}$$

$$\tilde{i}(4)' = \tilde{i}(5) \tag{18}$$

$$\tilde{i}(5)' = \tilde{i}(6) \tag{19}$$

$$\tilde{i}(6)' = \frac{\beta}{(1+\beta)} \left[c\,\tilde{i}(5)^2 - \left\{ \tilde{i}(1) + c\,\tilde{i}(4) \right\} \tilde{i}(6) + M\, \tilde{i}(5) + \beta\, K_1 \left(1 + \frac{1}{\beta}\right) \tilde{i}(5) \right] \tag{20}$$

$$\tilde{i}(7)' = \tilde{i}(8) \tag{21}$$

$$\tilde{i}(8)' = -Pr \left[\left\{ \tilde{i}(1) + c\,\tilde{i}(4) \right\} \tilde{i}(8) + Nb\, \tilde{i}(8)\, \tilde{i}(10) + Nt\, \tilde{i}(8)^2 \right] \tag{22}$$

$$\tilde{i}(9)' = \tilde{i}(10) \tag{23}$$

$$\tilde{i}(10)' = -Le\, Pr \left\{ \tilde{i}(1) + c\,\tilde{i}(4) \right\} \tilde{i}(10) - \left(\frac{Nt}{Nb} \right) \tilde{i}(8)' \tag{24}$$

Where

$$\begin{aligned} f &= \tilde{i}(1), \quad f' = \tilde{i}(2), \quad f'' = \tilde{i}(3), \quad f''' = \tilde{i}(3)', \\ g &= \tilde{i}(4), \quad g' = \tilde{i}(5), \quad g'' = \tilde{i}(6), \quad g''' = \tilde{i}(6)', \\ \Theta &= \tilde{i}(7), \quad \Theta' = \tilde{i}(8), \quad \Theta'' = \tilde{i}(8)' \\ \Phi &= \tilde{i}(9), \quad \Phi' = \tilde{i}(10), \quad \Phi'' = \tilde{i}(10)' \end{aligned} \tag{25}$$

4. Results and Discussion

Table 1 presents outcomes for $-\Theta'(0)$ when compared with Abolbashari et al. [30] and Gorla and Sidawi [31] for prominent values of Prandtl number Pr along with the residual errors. It is observed from the table that results obtained from the numerical simulation are highly accurate and have very little residual error. Results for $f''(0)$ and $g''(0)$ for variable in the values of stretching ratio parameter ranging from $0.0 - 8.0$ and Casson fluid parameter ranging from $0.1 - 0.9$ when $K = 0.1, M = 1.5, Pr = 0.73, Nb = 0.1, Nt = 0.5, Le = 2.0$ are shown in Table 2.

Table 1: Results for $-\Theta'(0)$ with variation in Pr: A comparison

Pr	Abolbashari et al. [30]	Residual Error	Gorla and Sidawi [31]	Residual Error	Present result
2	0.9114	-0.00055	0.9114	-0.00055	0.91135
7	1.8905	0.00000	1.8954	-0.00490	1.89540
20	-	-	3.3539	0.00000	3.35390
70	-	-	6.4622	0.00001	6.46219

Table 2: Results for c and β with $K = 0.1, M = 1.5, Pr = 0.73, Nb = 0.1, Nt = 0.5, Le = 2.0$

c	β	$f''(0)$	$g''(0)$
0.0	0.1	-0.572112	-0.51645943
2.0		-0.624727	-0.671375152
4.0		-0.672729	-0.79608024
6.0		-0.717334	-0.90349963
8.0		-0.759231	-0.999325368
2.0	0.1	-0.624727	-0.671375152
	0.3	-0.915383	-0.995627838
	0.5	-1.079947	-1.178022181
	0.7	-1.190544	-1.300354577
	0.9	-1.271079	-1.389345923

Table 3: Values of $Nu_x Re_x^{-1/2}$ for variables Nb, Pr

Nb	Pr	$Nu_x Re_x^{-1/2}$
2	0.73	0.33065
4		0.10494
6		0.03034
8		0.00828
10		0.00218
0.1	0.1	0.28959
	0.2	0.44883
	0.3	0.56678
	0.4	0.65905
	0.5	0.73401

Table 4: Values of $Sh_x Re_x^{-1/2}$ for variables Pr, Nt, Nb, Le

Pr	Nt	Nb	Le	$Sh_x Re_x^{-1/2}$
0.1	0.5	0.1	2.0	-0.37389
0.2				-0.46996
0.3				-0.48351
0.4				-0.46462
0.5				-0.42381
0.73	1			-1.31182
	1.5			-1.80865
	2			-1.92854
	2.5			-1.79595
	3			-1.50237
	0.5	0.01		-17.92028
		0.02		-8.11443
		0.03		-4.84604
		0.04		-3.21201
		0.05		-2.23173
		0.1	1	-1.32196
			2	-0.27216
			3	0.39794
			4	0.90612
			5	1.32325

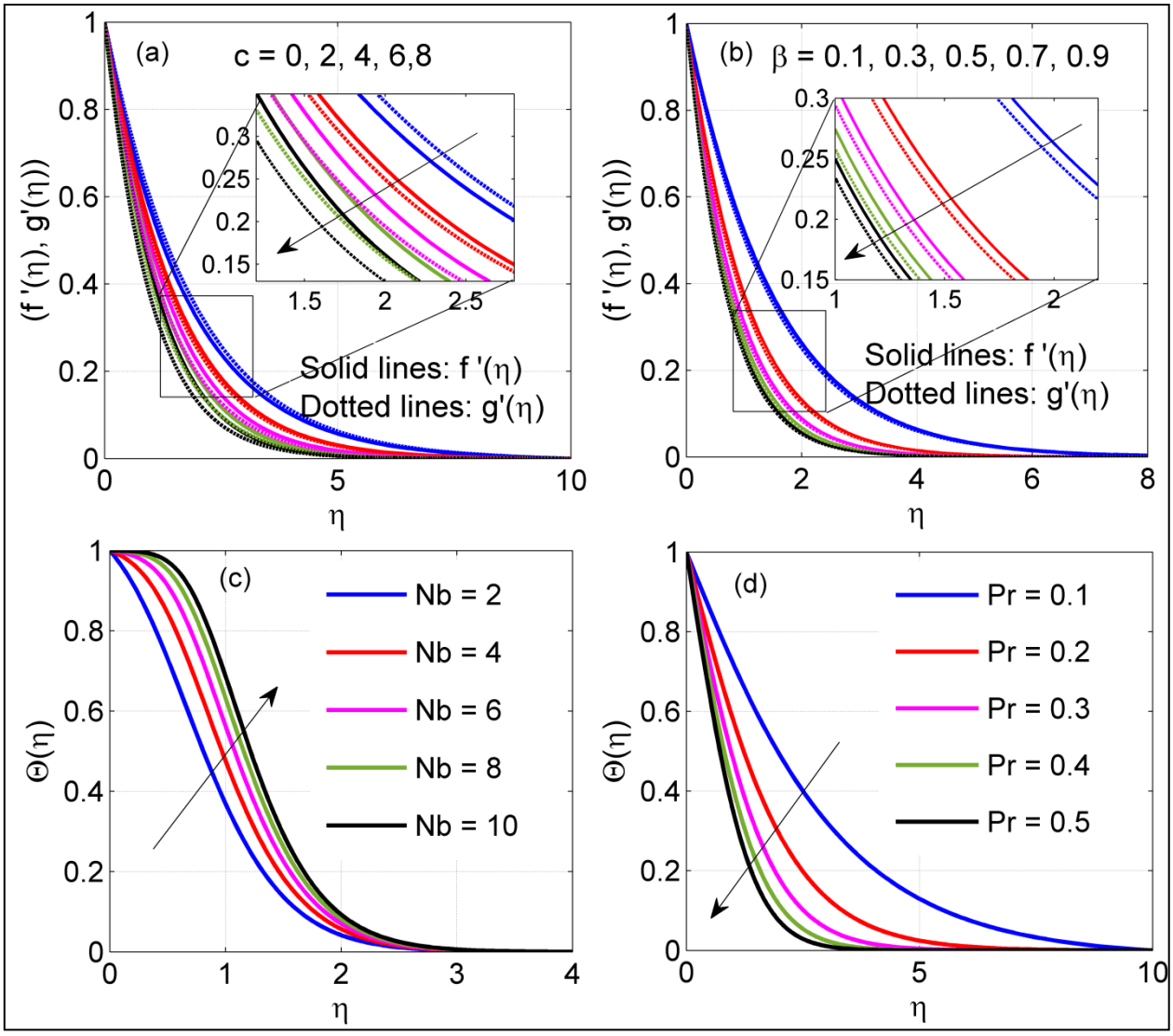

Fig. 2: (a) Velocity profile for c, (b) Velocity profile for β, (c) Temperature profile for Nb and (d) Temperature profile for Pr.

Also, Table 3 shows the values of $Nu_x Re_x^{-1/2}$ against Nb ($2.0 \leq Nb \leq 10.0$) and Pr ($0.1 \leq Pr \leq 0.5$) with fixed values of parameters as $c = 2.0, K = \beta = 0.1, M = 1.5, Nt = 0.5, Le = 2.0$. Furthermore, Table 4 displayed the numerical values of $Sh_x Re_x^{-1/2}$ against crucial parameters Pr, Nt, Nb and Le when $c = 2.0, K = \beta = 0.1, M = 1.5$. Figure 2 comprises the graphical representation of horizontal and tangential velocity against parameters c ($0 \leq c \leq 8$), β ($0.1 \leq \beta \leq 0.9$) and temperature profile under the influence of Nb ($2 \leq Nb \leq 10$) and Pr ($0.1 \leq Pr \leq 0.5$). Figure 2(a) shows that non-dimensional velocity profile, $f'(\eta), g'(\eta)$ (shown by solid and dotted lines, respectively) against stretching ratio parameter c and $f'(\eta), g'(\eta)$ declines for higher c. Variation in $f'(\eta), g'(\eta)$ under the impact of Casson parameter has been displayed in Figure 2(b). Since the fluid is non-Newtonian thus, sheer stress is produced, which ultimately declines the velocity profile for higher values of β. Also, figure 2(c) represents the temperature field against controlling nanofluid parameter Nb and shows that $\theta(\eta)$ enhances with enhancement in Nb from $Nb = 2.0$ to $Nb = 10.0$. This is due to the random motion of nanoparticles produced by suspended particles that consequently raises the width of boundary layer. Furthermore, a graphical representation of temperature for the Prandtl number is shown in Figure 2(d). This figure elaborates that the temperature behavior of the Prandtl number is reversed to that of Nb, which is due to the declination of diffusion rate for higher Pr.

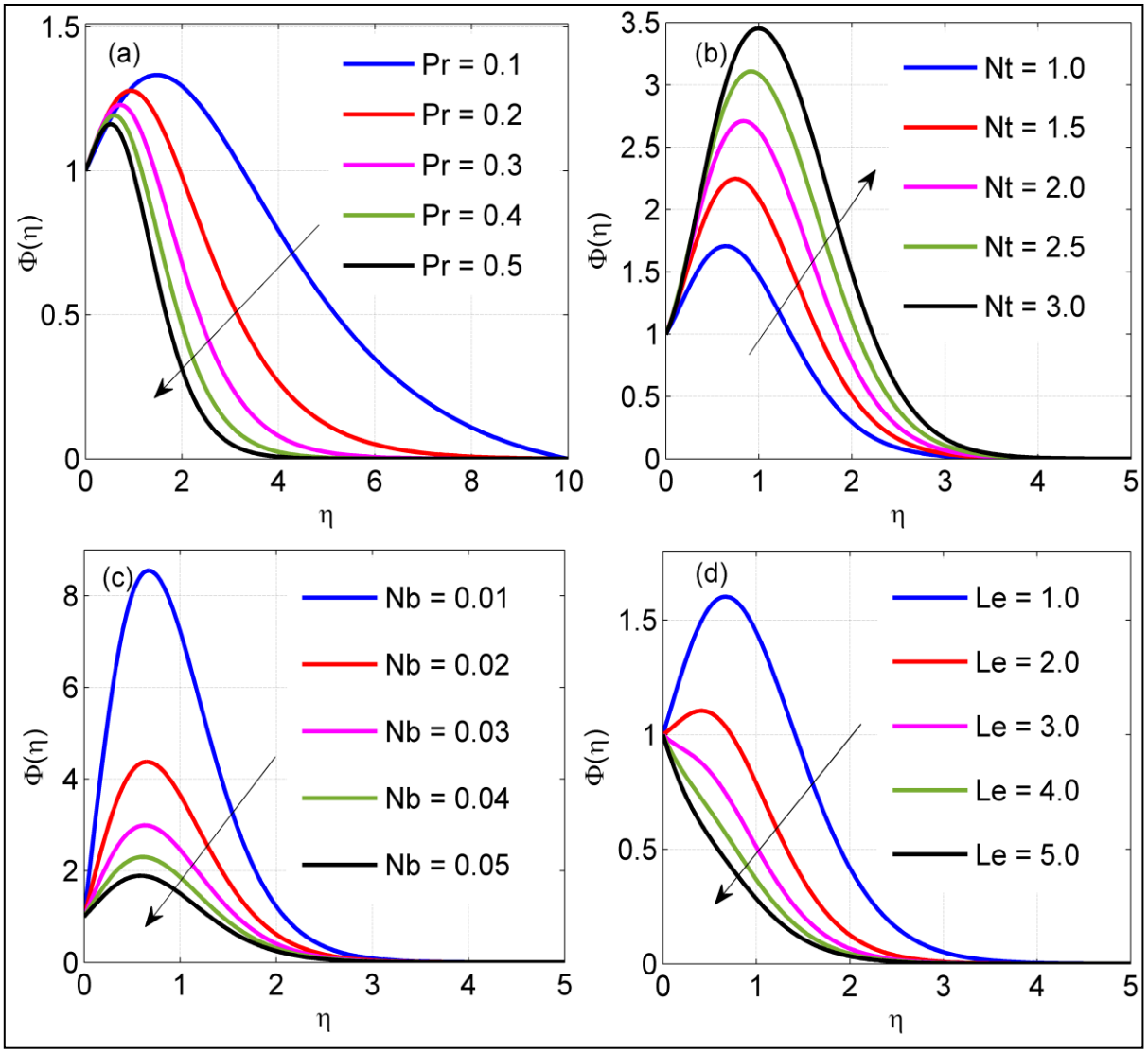

Fig. 3: (a) Concentration distribution for Pr, (b) Nt, (c) Nb and (d) Le.

Figure 3 shows the concentration distribution against Pr$(0.1 \leq Pr \leq 0.5)$,$Nt(1.0 \leq Nt \leq 3.0)$, $Nb(0.01 \leq Nb \leq 0.05)$ and Le $(1.0 \leq Le \leq 5.0)$. Figure 3(a) displays the impact of Pr over the concentration field. This figure shows that a higher Prandtl number Pr declines nanoparticle concentration due to a lower diffusivity value because diffusivity rate and Prandtl number are inversely proportional to each other. Variation in $\Phi(\eta)$ against nanofluid parameter thermophoresis is shown via Figure 3(b), and this graph represents that concentration rises with the rise in Nt. Consequently, the Sherwood number declines for higher Pr, which can be visualized in Table 4. Figure 3(c) portrays the variation in concentration profile under the impact of nanofluid parameter Nb. Higher Nb falls down boundary layer thicknesses that ultimately decrease nanoparticle concentration, as seen in Figure 3(c). Figure 3(d) displays the graphical representation for Lewis number over nanoparticle concentration, and it is noticed that $\Phi(\eta)$ decreases for more Le. Moreover, all plots of this figure fall distinctly upto $\eta = 4.0$ (approximately) when Le $(1.0 \leq Le \leq 5.0)$ and meets the convergence criterion.

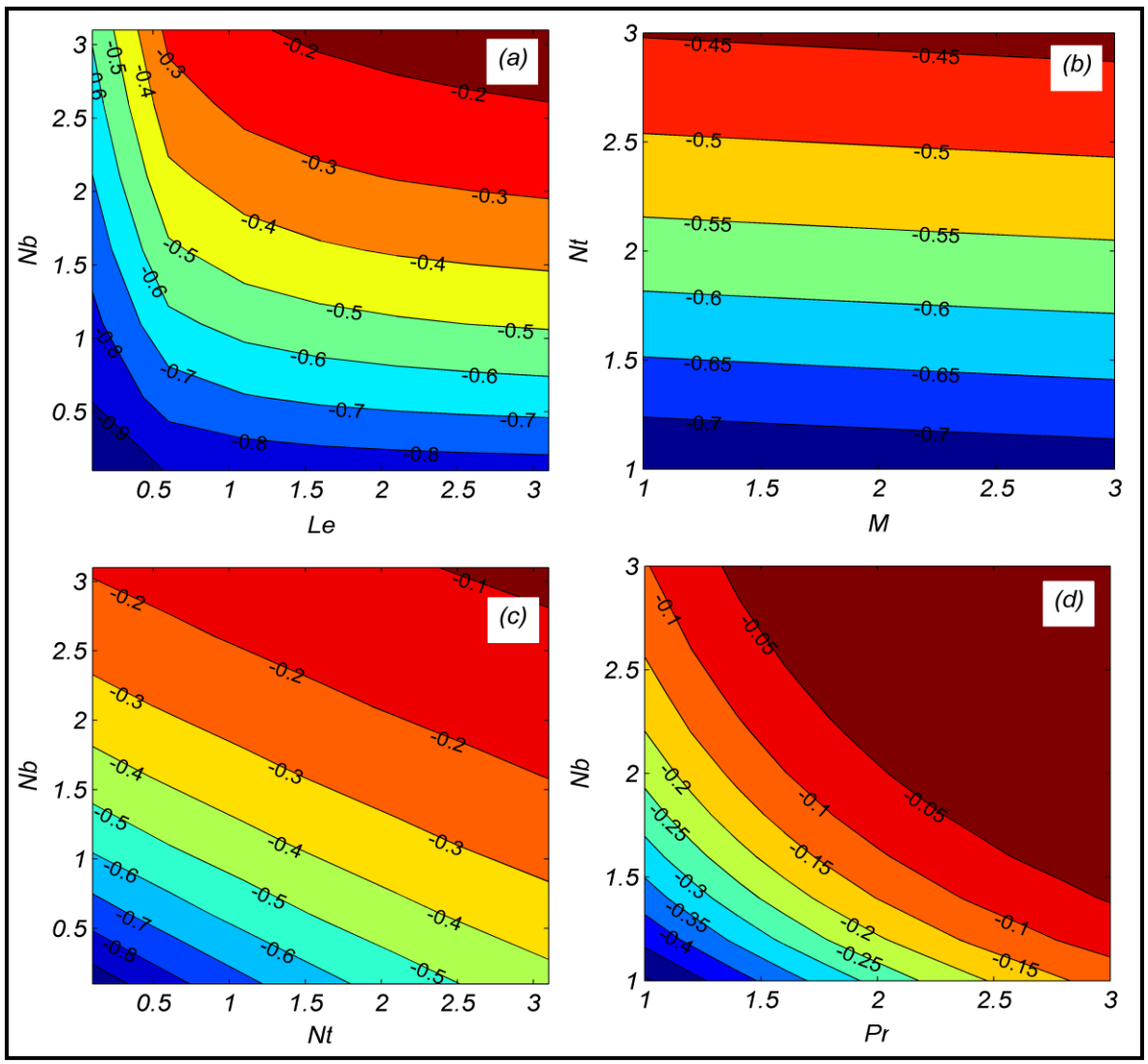

Fig. 4: Contour plots for Skin friction coefficient against (a) Le & Nb, (b) M & Nt, (c) Nt & Nb and (d) Pr & Nb when $C_r = 0.7, c = 2, K1 = 0.1, \beta = 0.1, M = 1.5, Pr = 0.73, Nb = 0.1, Nt = Le = 0.5$.

Figure 4(a)-4(d) shows the impact of skin friction under the influence of Le & Nb, M & Nt, Nt & Nb and Pr & Nb when $C_r = 0.7, c = 2, K1 = 0.1, \beta = 0.1, M = 1.5, Pr = 0.73, Nb = 0.1, Nt = Le = 0.5$ via contour plots. Skin friction coefficient augmented with augmentation in Le & Nb as visualized in Figure 4(a). Figure 4(b) manifests the impact of skin friction against $M(1 \leq M \leq 2)$ & $Nt(1 \leq M \leq 3)$, and it shows that for higher values of M & Nt, enhancement in value of skin friction has been noticed. The same impact of skin friction when a rise in values of Nt & Nb has been noticed, as presented in Figure 4(c). Figure 4(d) illustrates skin friction against Pr & Nb. For higher $Pr(1 \leq Pr \leq 3)$& $Nb(1 \leq Nb \leq 3)$, skin friction coefficient rises up as shown in Figure 4(d). Figure 5(a)-5(d) shows impact of Nusselt number $Nu_x Re_x^{-1/2}$ against Nb & c, Nb & Le, Nb & Nt and Nb & Pr respectively. In Figure 5(a), $Nu_x Re_x^{-1/2}$ enhances with a rise in Nb but declines when there is an increase in Nb and $c(2.5 \leq c \leq 4.5)$. Impact of $Nu_x Re_x^{-1/2}$ against $Nb(1.0 \leq Nb \leq 3.0)$ for different $Le(1.0, 1.2, 1.4, 1.6, 1.8)$ has been visualized in Figure 5(b). This plot shows that $Nu_x Re_x^{-1/2}$ falls with a rise in both Nb & Le. Figure 5(c) and 5(d) manifests influence of $Nu_x Re_x^{-1/2}$ over Nb & Nt and Nb & Pr respectively. Both the plots show Nusselt number, $Nu_x Re_x^{-1/2}$ declines with a rise in

Nb $(1.0 \leq Nb \leq 3.0)$ & $Nt(0.1, 0.2, 0.3, 0.4, 0.5)$ and $Nb(1.0 \leq Nb \leq 3.0)$ & Pr $(1, 2, 3, 4, 5)$ as visualized in Figure 5(c) and 5(d) serially.

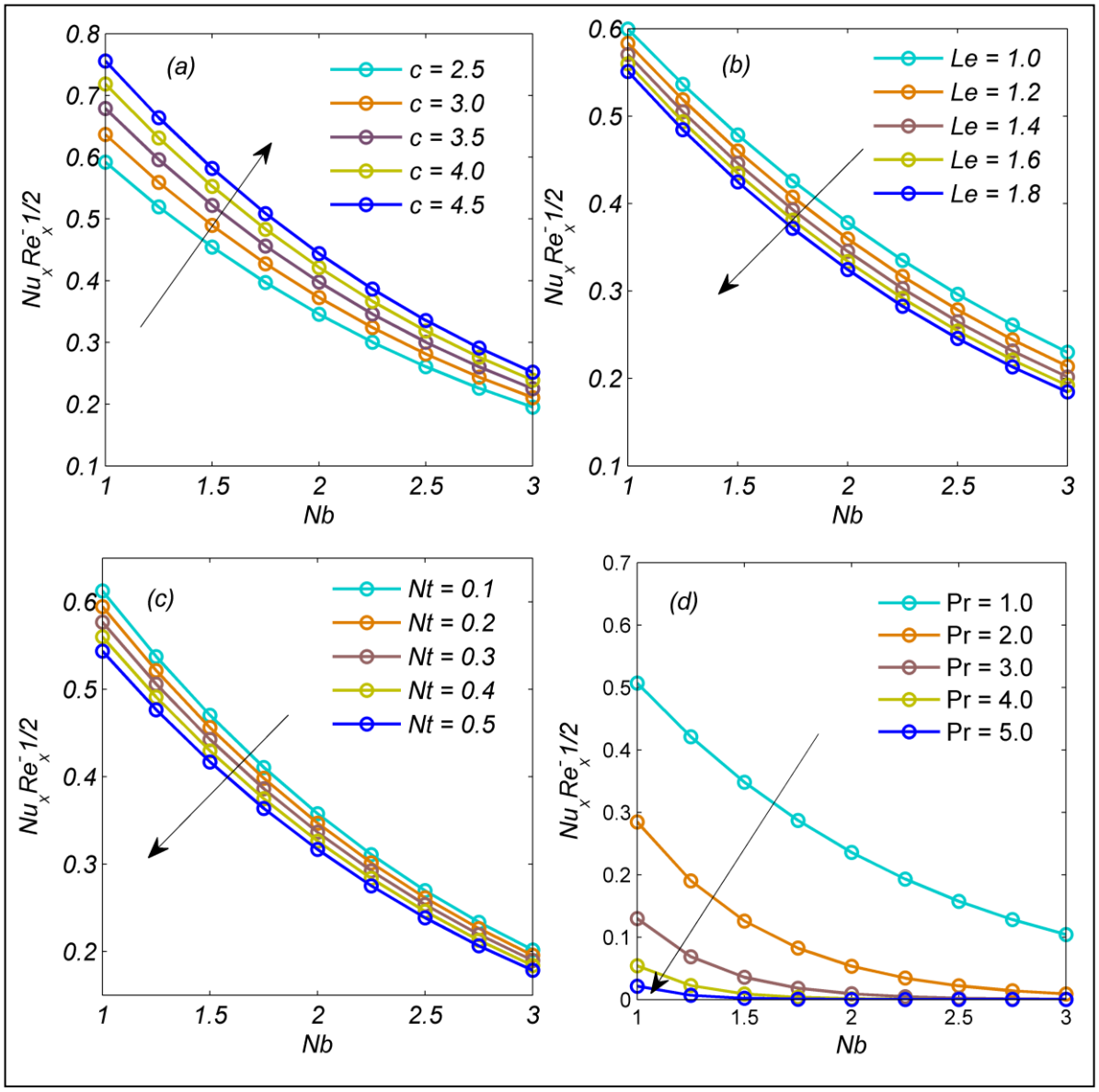

Fig. 5: Nusselt number against a) Nb & c, (b) Nb & Le, (c) Nb & Nt and (d) Nb & Pr.

5. Conclusion

This study has considered three-dimensional magnetohydrodynamic flows in non-Newtonian nanofluids over permeable stretching surfaces. Final results and residual errors are compared with Abolbashari et al. [30] and Gorla and Sidawi [31]. Good agreement regarding the convergence criterion has been observed. The main fallout of current research are:

- Brownian motion parameter Nb amplifies temperature distribution whereas higher Prandtl number Pr lessens temperature profile.
- Velocity profiles (horizontal and tangential) decline for higher stretching ratio parameter c and Casson fluid parameter β.

- Augmentation in Pr, Nb, and Le will help to decline the concentration of the nanofluids while higher thermophoresis reverses the impact on concentration due to temperature gradient and mass flux.

The resulting outcomes of the current research help the technological, biological, and manufacturing fields produce the desired product. Additionally, recent research can be extended by adding gyrotactic micro-organisms with Stefan blowing impact in non-Newtonian nanofluids over different geometries.

Nomenclature:

x, y, z	Coordinate axes
ν	Kinematic viscosity
β	Casson parameter
σ	Electrical conductivity
k_1	Permeability parameter
u, v	Velocity components
C_∞	Ambient concentration
T_∞	Ambient temperature
C_r	Non-dimensional chemical reaction parameter
Nt	Thermophoresis parameter
Pr	Prandtl number
D_T	Thermophoresis diffusion coefficient
k	Thermal conductivity
D_B	Brownian diffusion coefficient
Sh_x	Sherwood number
Le	Lewis number
η	Similarity variable
a, b, c	Constants
C	Concentration
T	Temperature
C_w	Wall Concentration
Nu_x	Nusselt number
T_w	Wall temperature
$\left(\rho C_p\right)_f$	Heat capacity of the fluid
M	Magnetic parameter
K_1	Permeability parameter
Cf_x, Cf_y	Axial and transverse skin friction coefficients
Re_x	Reynolds number

$\left(\rho C_p\right)_p$	Heat capacity of the particle

Refrences

[1] Shafiq, A., Rasool, G., Khalique, C. M., & Aslam, S. (2020). Second grade bioconvective nanofluid flow with buoyancy effect and chemical reaction. *Symmetry*, *12*(4), 621.

[2] Ibrahim, W., & Anbessa, T. (2020). Three-dimensional MHD mixed convection flow of Casson nanofluid with hall and ion slip effects. *Mathematical Problems in Engineering*, *2020*.

[3] Rana, P., Gupta, S., & Gupta, G. (2022). Unsteady nonlinear thermal convection flow of MWCNT-MgO/EG hybrid nanofluid in the stagnation-point region of a rotating sphere with quadratic thermal radiation: RSM for optimization. *International Communications in Heat and Mass Transfer*, *134*, 106025.

[4] Goyal, R., Vinita, Sharma, N., & Bhargava, R. (2021). GFEM analysis of MHD nanofluid flow toward a power-law stretching sheet in the presence of thermodiffusive effect along with regression investigation. *Heat Transfer*, *50*(1), 234-256.

[5] Rana, P., Gupta, S., & Gupta, G. (2023). Optimization of heat transfer by nonlinear thermal convection flow past a solid sphere with Stefan blowing and thermal slip using Taguchi method. *International Communications in Heat and Mass Transfer*, *141*, 106580.

[6] Gupta, S., Kumar, D., & Singh, J. (2019). Magnetohydrodynamic three-dimensional boundary layer flow and heat transfer of water-driven copper and alumina nanoparticles induced by convective conditions. *International Journal of Modern Physics B*, *33*(26), 1950307.

[7] Gireesha, B. J., Kumar, K. G., Rudraswamy, N. G., & Manjunatha, S. (2018). Effect of viscous dissipation on three dimensional flow of a nanofluid by considering a gyrotactic microorganism in the presence of convective condition. In *Defect and Diffusion Forum* (Vol. 388, pp. 114-123). Trans Tech Publications Ltd.

[8] Rana, P., Kumar, A., & Gupta, G. (2022). Impact of different arrangements of heated elliptical body, fins and differential heater in MHD convective transport phenomena of inclined cavity utilizing hybrid nanoliquid: Artificial neutral network prediction. *International Communications in Heat and Mass Transfer*, *132*, 105900.

[9] Rana, P., & Khurana, M. (2023). Linear and weakly nonlinear investigation in thermal stability analyses of MHD convection utilizing non-Newtonian nanofluid in rotating frame of reference. *Waves in Random and Complex Media*, 1-27.

[10] Nayak, M. K., Akbar, N. S., Tripathi, D., & Pandey, V. S. (2017). Three dimensional MHD flow of nanofluid over an exponential porous stretching sheet with convective boundary conditions. *Thermal Science and Engineering Progress*, *3*, 133-140.

[11] Rana, P. (2020, March). MHD convective heat transfer in the annulus between concentric cylinders utilizing nanoparticles and non-uniform heating. In AIP Conference Proceedings (Vol. 2214, No. 1). AIP Publishing

[12] Rao, P. S., Prakash, O., Mishra, S. R., & Sharma, R. P. (2020). Similarity solution of three-dimensional MHD radiative Casson nanofluid motion over a stretching surface with chemical and diffusion-thermo effects. *Heat Transfer*, *49*(4), 1842-1862.

[13] Nayak, M. K., Prakash, J., Tripathi, D., Pandey, V. S., Shaw, S., & Makinde, O. D. (2020). 3D Bioconvective multiple slip flow of chemically reactive Casson nanofluid with gyrotactic micro-organisms. *Heat Transfer—Asian Research*, *49*(1), 135-153.

[14] Ramzan, M., Inam, S., & Shehzad, S. A. (2016). Three dimensional boundary layer flow of a viscoelastic nanofluid with Soret and Dufour effects. *Alexandria Engineering Journal*, *55*(1), 311-319.

[15] Mallikarjuna, H. B., Jayaprakash, M. C., & Mishra, R. (2019). Three-dimensional boundary layer flow and heat transfer of a fluid particle suspension over a stretching sheet embedded in a porous medium. *Nonlinear Engineering*, *8*(1), 734-743.

[16] Ramamoorthy, M., & Pallavarapu, L. (2020). Radiation and Hall effects on a 3D flow of MHD Williamson fluid over a stretchable surface. *Heat Transfer*, *49*(8), 4410-4426.

[17] Khan, M. N., Nadeem, S., Ullah, N., & Saleem, A. (2020). Theoretical treatment of radiative Oldroyd-B nanofluid with microorganism pass an exponentially stretching sheet. *Surfaces and Interfaces*, *21*, 100686.
[18] Makkar, V., Poply, V., Goyal, R., & Sharma, N. (2021). Numerical Investigation of MHD Casson Nanofluid Flow towards a non-linear Stretching Sheet in presence of Double-Diffusive effects along with Viscous and Ohmic Dissipation. *Journal of Thermal Engineering*, *7*(2), 1-17.
[19] Magagula, V. M., Shaw, S., & Kairi, R. R. (2020). Double dispersed bioconvective Casson nanofluid fluid flow over a nonlinear convective stretching sheet in suspension of gyrotactic microorganism. *Heat Transfer*, *49*(5), 2449-2471.
[20] Gireesha, B. J., Archana, M., Prasannakumara, B. C., Gorla, R. R., & Makinde, O. D. (2017). MHD three dimensional double diffusive flow of Casson nanofluid with buoyancy forces and nonlinear thermal radiation over a stretching surface. *International Journal of Numerical Methods for Heat & Fluid Flow*.
[21] Al-Khaled, K., & Khan, S. U. (2020). Thermal aspects of Casson nanoliquid with gyrotactic microorganisms, temperature-dependent viscosity, and variable thermal conductivity: bio-technology and thermal applications. *Inventions*, *5*(3), 39.
[22] Ganesh Kumar, K. (2019). Scrutinization of 3D flow and nonlinear radiative heat transfer of non-Newtonian nanoparticles over an exponentially sheet. *Int J Numer Methods Heat Fluid Flow*, *30*(4), 2051-2062.
[23] Rana, P., Kumar, A., & Gupta, G. (2022). Impact of different arrangements of heated elliptical body, fins and differential heater in MHD convective transport phenomena of inclined cavity utilizing hybrid nanoliquid: Artificial neutral network prediction. *International Communications in Heat and Mass Transfer*, *132*, 105900.
[24] Megahed, A. M. (2019). Williamson fluid flow due to a nonlinearly stretching sheet with viscous dissipation and thermal radiation. *Journal of the Egyptian Mathematical Society*, *27*(1), 1-10.
[25] Rana P. Heat transfer optimization and rheological features of Buongiorno nanofluid in a convectively heated inclined annulus with nonlinear thermal radiation. *Propulsion and Power Research*. 2023 Dec 1;12(4):539-55.
[26] Buongiorno, J. (2006). Convective transport in nanofluids. *Journal of Heat Transfer, 128*, 240-250.
[27] Shateyi, S. (2017). Numerical analysis of three-dimensional MHD nanofluid flow over a stretching sheet with convective boundary conditions through a porous medium. *Nanofluid Heat Mass Trans. Eng. Problems*.
[28] Khan, J. A., Mustafa, M., Hayat, T., & Alsaedi, A. (2015). Three-dimensional flow of nanofluid over a non-linearly stretching sheet: An application to solar energy. *International Journal of Heat and Mass Transfer*, *86*, 158-164.
[29] Sulochana, C., Ashwinkumar, G. P., & Sandeep, N. (2016). Similarity solution of 3D Casson nanofluid flow over a stretching sheet with convective boundary conditions. *Journal of the Nigerian Mathematical Society*, *35*(1), 128-141.
[30] Abolbashari, M. H., Freidoonimehr, N., Nazari, F., & Rashidi, M. M. (2015). Analytical modeling of entropy generation for Casson nano-fluid flow induced by a stretching surface. *Advanced Powder Technology*, *26*(2), 542-552.
[31] Gorla, R. S. R., & Sidawi, I. (1994). Free convection on a vertical stretching surface with suction and blowing. *Applied Scientific Research*, *52*(3), 247-257.